


RESEARCH ARTICLE | MAY 04 2023

Toward in-fiber nonlinear silicon photonics

Li Shen ; Meng Huang; Shiyu Sun; ... et. al



APL Photonics 8, 050901 (2023)

<https://doi.org/10.1063/5.0148117>



View
Online



Export
Citation

CrossMark

Articles You May Be Interested In

Continuous-wave Raman amplification in silicon core fibers pumped in the telecom band

APL Photonics (September 2021)

Measuring the timeline of retroactive sentence repair

J Acoust Soc Am (March 2023)

Sliding window correlation analysis for dengue-climate variable relationship

AIP Conference Proceedings (November 2016)

APL Photonics

Special Topic: State-of-the-art and Future
Directions in Optical Frequency Combs

Submit Today!

Toward in-fiber nonlinear silicon photonics

Cite as: APL Photon. 8, 050901 (2023); doi: 10.1063/5.0148117

Submitted: 28 February 2023 • Accepted: 12 April 2023 •

Published Online: 4 May 2023



Li Shen,^{1,a)}  Meng Huang,² Shiyu Sun,² Dong Wu,²  Zhiwei Yan,¹  Haonan Ren,^{2,b)}
and Anna C. Peacock^{2,a)} 

AFFILIATIONS

¹ Wuhan National Laboratory for Optoelectronics and School of Optical and Electronic Information, Huazhong University of Science and Technology, Wuhan 430074, Hubei, China

² Optoelectronics Research Centre, University of Southampton, Southampton SO17 1BJ, United Kingdom

^{a)} Authors to whom correspondence should be addressed: lishen@hust.edu.cn and acp@orc.soton.ac.uk

^{b)} Now at: School of Optoelectronic Engineering and Instrumentation Science, Dalian University of Technology, Dalian 116024, China.

ABSTRACT

Silicon core fibers (SCFs) offer an exciting opportunity to harness the nonlinear functionality of the semiconductor material within the excellent waveguiding properties of optical fiber systems. Over the past two decades, these fibers have evolved from a research curiosity into established components for use across a wide range of photonic applications. This article provides a comprehensive overview of the evolution of the SCFs, with a focus on the development of the fabrication and post-processing procedures that have helped unlock the nonlinear optical potential of this new technology. As well as reviewing the timeline of advancements in nonlinear performance, a perspective will be provided on the current challenges and future opportunities for in-fiber nonlinear silicon systems.

© 2023 Author(s). All article content, except where otherwise noted, is licensed under a Creative Commons Attribution (CC BY) license (<http://creativecommons.org/licenses/by/4.0/>). <https://doi.org/10.1063/5.0148117>

I. INTRODUCTION

Silicon is one of the most important materials of our time. As well as being a long-standing workhorse in the microelectronics industry, over the past two decades, it has proven itself as an excellent platform for a myriad of optical technologies spanning traditional communications to sensing and spectroscopy.^{1,2} An important branch of active silicon research covers nonlinear photonics, where the aim is to make use of silicon's large intrinsic, ultrafast nonlinearities to intricately control and manipulate light with light.³ To this end, nonlinear processes in silicon have been widely studied, resulting in several significant device demonstrations, including high-speed, high-density all-optical processing,⁴ octave-spanning frequency comb generation,⁵ and Raman lasing.⁶ Owing to the advanced fabrication technologies that have been developed for CMOS processing, the majority of the work in this field has made use of planar waveguides fabricated from the silicon-on-insulator (SOI) platform. Although these planar waveguides present an exciting opportunity for integrated photonic systems, they do suffer from some drawbacks. For example, their small dimensions, typically nanometer-sized, can limit their power handling capabilities, restrict their wavelength coverage to the near-infrared regime, and

make robust integration with optical fiber connectors challenging and alignment sensitive.

An alternative waveguide platform that offers an elegant solution to these issues is the emerging class of silicon core fibers (SCFs). Notably, SCFs are principally fabricated using conventional fiber drawing methods, which allow for the rapid production of long lengths of fiber at low cost.⁷ Moreover, as the SCFs are still clad in silica, they retain many of the benefits of conventional fiber technologies, such as robustness, stability, and compatibility with standard fiber post-processing methods such as tapering and splicing. Significantly, it is the ability to post-process the SCFs following the initial drawing phase that has allowed for the greatest advances in terms of their use for nonlinear applications. For example, fiber tapering provides a means to adjust the core size from a few micrometers down to hundreds of nanometers in diameter so that the fibers can be tailored to operate over a broad range of wavelengths and powers.⁸ Moreover, the heat treatments also provide a route to reducing the transmission and coupling losses through reshaping and recrystallizing of the core.⁹

Accordingly, this article presents an overview of the SCF technology, with a focus on the exploitation of post-processing procedures for optimization of nonlinear performance. In addition to

reviewing the current state of the art, we will also provide some perspective as to where the SCFs offer significant benefits in terms of their flexibility, power handling, wavelength coverage, and general ease of use over competing platforms.

II. THE HISTORY OF SILICON CORE FIBERS

A. Silicon core fibers fabrication and post-processing

The first report on SCFs for use in optical applications appeared in 2006.¹⁰ The motivation for this work was to combine the unique optoelectronic properties of the semiconductor material with the excellent light guiding properties of fiber waveguides. The fibers presented in this work were produced by depositing the silicon materials inside the pores of silica capillaries and microstructured fibers via a high-pressure chemical vapor deposition (HPCVD) technique, as shown in the schematic of Fig. 1(a). Significantly, by tuning the temperature of the deposition, this technique allows for the fabrication of SCFs with both amorphous and polycrystalline core materials. Subsequent to these efforts, an alternative production method for SCFs based on a modified form of traditional fiber drawing was presented in 2008.⁷ In this approach, the silicon core was simply sleeved inside a silica glass cladding tube to create a preform before being drawn down to fiber dimensions, as illustrated in Fig. 1(b). However, as the silicon core is molten at the draw temperature for silica ($\sim 1950^\circ\text{C}$), this method was called the molten core method (MCM), and the high processing temperatures ensure that the core materials are always produced in a polycrystalline phase. Importantly, thanks to the excellent stability and strong viscosity of silica, the cladding tube acts as a crucible to contain the molten semiconductor, allowing for long lengths of continuous fiber to be produced in a single draw process.

In the decade following the SCF's inception, much work was conducted by the fabrication teams, both HPCVD and MCM, to advance the production methods, including investigating the role of the core shape¹¹ and size.¹² One of the most notable advancements was the inclusion of interface modifiers for the MCM produced fibers, as illustrated by the CaO coating in Fig. 1(b), which helped alleviate issues with oxygen diffusion and the thermal mismatch of the core/cladding materials during the high temperature processing.¹³ Despite such efforts, the SCFs were still typically produced with relatively high transmission losses, within the range of 3–10 dB/cm in the telecom band,¹⁴ restricting the fiber lengths that could be used in optical and, more specifically, nonlinear optical applications. This is particularly pronounced for SCFs fabricated with the smallest core dimensions due to the challenges involved in their production, such as the mass transport of materials for the HPCVD method and Rayleigh instabilities for the MCM fibers. As a result,

various forms of post-processing procedures have been explored, including thermal annealing,¹⁵ fiber tapering,^{8,16} and laser crystallization.¹⁷ In all cases, the aim of the post-process is to melt and crystallize the core to reduce the impurities and increase the grain sizes of the polycrystalline material. We note that such post-processing is only suitable for obtaining crystalline cores due to the instability of the amorphous materials, and consequently, it is the crystalline core fibers that have become the most developed SCFs in recent times.

Of the post-processing methods, fiber tapering has become the most useful and widely employed approach. This is because tapering involves both the heating and stretching of the fiber, as illustrated in Fig. 1(c), so that it is possible to simultaneously control both the diameter and the crystallinity of the fiber core. This is particularly important for nonlinear applications, as control of the core size allows for tailoring of the dispersion and nonlinearity parameters,¹⁸ while controlling the cooling rate of the processed core can result in increased grain sizes⁹ and thus significantly reduced losses (~ 1 dB/cm in $\sim 1\ \mu\text{m}$ core diameter fibers).¹⁹ Moreover, by adjusting the tapering profile, it is also possible to control the longitudinal dimensions of the fiber, which can be exploited to enhance the coupling regions and/or alter the dispersion to tune the efficiency of the various nonlinear processes along the propagation length. To access SCFs with submicron-sized cores, which are favored for nonlinear processing at telecom wavelengths, a two-step tapering process has been developed. Importantly, by using the first step to reduce the SCF outer diameter, a lower filament power can be used in the second taper step, which allows for the production of continuous cores of sub-micrometer dimensions with large crystalline grains and reduced residual stress. Although the submicron SCF lengths are currently limited to a few centimeters due to the constraints of our tapering rig, these are sufficient for most nonlinear applications, thanks to the high nonlinearity of silicon.

Somewhat related to the draw then taper approach to SCF fabrication, more recently, an alternative two-step drawing method has been developed that can produce even longer lengths of low loss SCFs, as indicated by the schematic in Fig. 1(d).²⁰ The starting point of this process is to create a preform that consists of a silicon rod inserted into a microstructured stack of silica capillaries, and thus this method has been called the rod-in-stack method. The preform is then drawn into a cane, which is then sleeved into a single capillary tube before a second draw takes place to produce the fiber. This second draw stage thus mimics the post-draw tapering to some degree, as it provides a means to reprocess the silicon core to obtain micrometer dimensions with a well-ordered crystalline structure. Significantly, this method has produced the longest lengths of low loss fiber to date (0.2 dB/cm over a 1 m length of a $3\ \mu\text{m}$ core fiber),

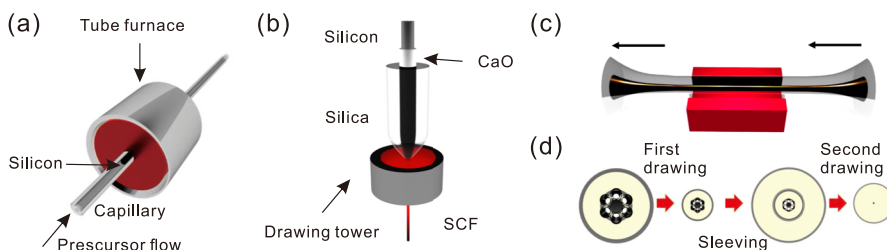


FIG. 1. Schematic of the SCF fabrication and post-processing methods. (a) High-pressure chemical vapor deposition (HPCVD) technique. (b) Molten core method (MCM) of fiber drawing. (c) Post-processing via tapering. (d) Two-step drawing via the rod-in-stack fabrication method.

though so far, nonlinear propagation has yet to be demonstrated in these SCFs.

Although less developed, it is worth highlighting some of the advancements that have been made in the laser processing of SCFs. Laser heat treatments have been successfully applied to increase the crystal grain size in the silicon core and thus reduce the transmission losses,¹⁷ as well as to introduce localized strain into the core to tune the bandgap energy,²¹ albeit over shorter processing lengths than the tapering or drawing methods. However, an area where this method potentially shows greater promise is in the processing of fibers with compound semiconductor cores (e.g., SiGe²² and GaAs²³), where localized heating can be used to precisely control the composition of the material. As these fibers are not the focus of this article, more details on the laser processing of compound core materials can be found in the relevant literature.²⁴

To highlight the progress made in the fabrication and post-processing of the SCFs to date, Fig. 2(a) plots a map of the SCF transmission loss, as measured in the telecom C-band, as a function of core diameter for fibers produced via the different methods.^{9,10,14,16,17,25–30} Critical to observing nonlinear propagation has been the production of SCFs with losses <3 dB/cm, something that has been achieved in both the amorphous and polycrystalline core fibers. Significantly, the lowest losses are now routinely <3 dB/cm in a few micrometer sized SCF cores, which is comparable to the lowest reported losses obtained in planar waveguides.³¹ However, of similar importance has been the production of SCFs with core diameters of $\sim 1 \mu\text{m}$, as the smaller cores not only result in higher confinement of the light but also allow for waveguide dispersion tailoring, as illustrated in Fig. 2(b). Specifically, Fig. 2(b) shows

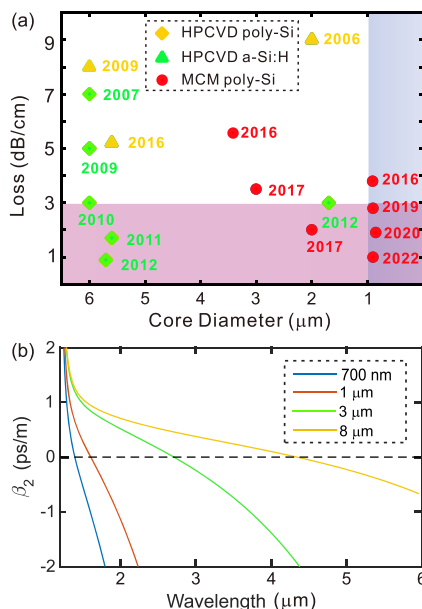


FIG. 2. (a) Recent progress to reduce the losses and core diameter in SCFs fabricated by both the HPCVD and MCM approaches. Shaded regions are a guide to indicate the production of SCFs with core diameters <1 μm and losses <3 dB/cm. (b) Dispersion tuning as a result of scaling the fiber core diameter, as labeled in the legend. The dashed line represents the zero-dispersion wavelength.

that, owing to the strong normal dispersion of silicon, SCF core diameters of <1 μm are required to access the anomalous dispersion regime in the telecoms band. Therefore, it is the recent developments in the tapering procedures to produce SCFs with a combination of low losses ($\sim 1 \text{ dB/cm}$) and submicron cores that have enabled many exciting demonstrations of nonlinear processing in this wavelength region. In fact, the smallest core SCF shown in Fig. 2(a) has a diameter of $\sim 700 \text{ nm}$, which also exhibits a low loss of $\sim 1 \text{ dB/cm}$.³⁰ We note that due to the high core/cladding index contrast of the SCFs, the fundamental mode is still well confined to the silicon core in the telecom band, even for diameters as small as $\sim 500 \text{ nm}$, allowing for further tailoring of the dispersion and nonlinear confinement as described in Ref. 8, and continued efforts to reduce the losses in these small core fibers will greatly enhance their practical use. However, it is important to mention that having access to low loss SCFs with larger, few micrometer cores is also very useful, particularly for applications that extend into the mid-infrared region, where there is a need to minimize the interaction of the long wavelength light with the lossy silica cladding, or alternatively for applications that require the use of high optical powers.

B. In-fiber nonlinear applications so far

There are a plethora of nonlinear processes available in silicon that arise from the interactions of the optical field with electrons and phonons. Owing to the centrosymmetry of the silicon materials, the second-order nonlinearity is not present, so nonlinear propagation in SCFs is dominated by third-order processes such as self-phase modulation (SPM), two-photon absorption (TPA), four-wave mixing (FWM), and Raman scattering (SRS). These processes can be used in a variety of applications, including all-optical modulation, wavelength conversion, amplification, signal regeneration, and more. Figure 3 presents a timeline of the nonlinear processes that have been observed in the SCFs, highlighting how the advancements made in terms of fabrication and post-processing have greatly expanded their application potential.

The first demonstrations of nonlinear propagation in the SCFs focused on characterizing the spectral broadening via SPM and nonlinear saturation due to TPA, as this provided a means to determine the nonlinear performance of the different core materials. This analysis revealed that the nonlinear refractive indices and the TPA parameters of the SCF cores, both hydrogenated amorphous (a-Si:H)²⁵ and polycrystalline (poly-Si),¹⁶ closely matched values reported for their planar waveguide counterparts, which was a good indication of the suitability of the core materials for nonlinear processing. However, as previously discussed, low linear losses are critical to observing high nonlinear efficiency, and thus it is only more recently that some key nonlinear processes have been reported. To illustrate this point, Fig. 4 presents two examples of SPM obtained in tapered SCFs when pumped with the same telecom band fiber laser (1540 nm center wavelength) that has a duration of 720 fs (FWHM) and a repetition rate of 40 MHz. The first spectrum in Fig. 4(a) was obtained using one of the first tapered SCFs, which had a core diameter of $\sim 1 \mu\text{m}$, a length of $\sim 1 \text{ cm}$, and a loss value of 3.5 dB/cm, where only a modest spectral broadening is obtained.¹⁶ The second spectrum in Fig. 4(b) was measured more recently in a submicron (0.9 μm) SCF with a waist length of 8 mm and a loss of 2.5 dB/cm. To ensure efficient coupling into the small core, the taper transitions

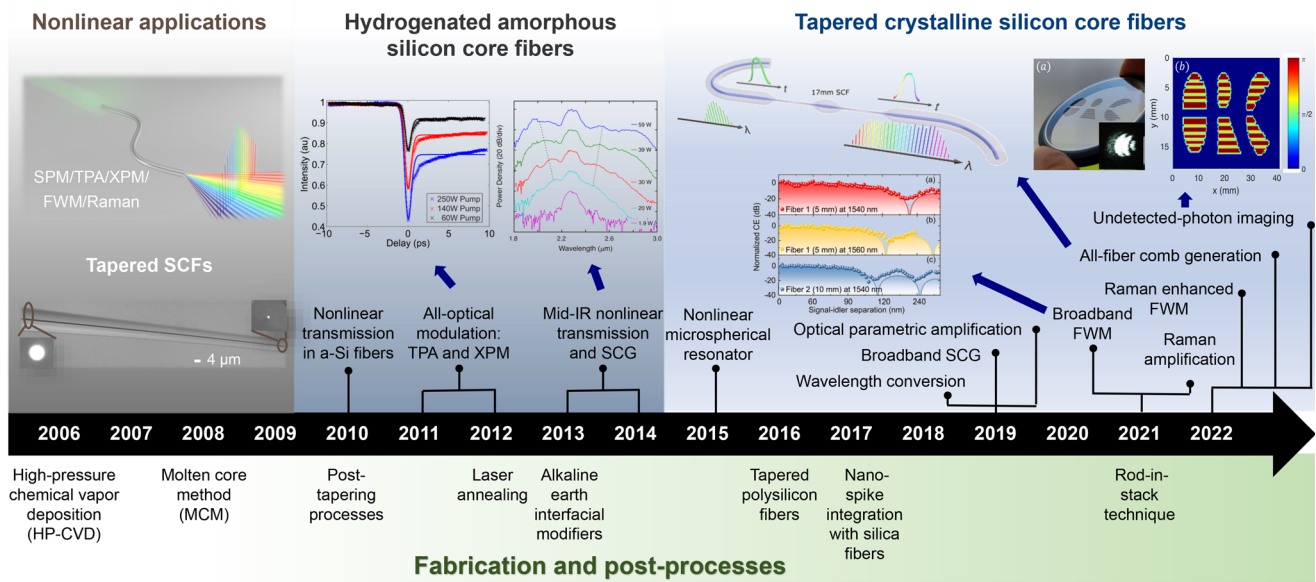


FIG. 3. Timeline of the evolution of SCFs. Lower half details the evolution of the fabrication and post-processing techniques representing a reduction in losses from left to right: HPCVD,¹⁰ MCM,⁷ post-tapering processes,⁸ laser annealing,⁶² alkaline earth interfacial modifiers,¹³ tapered poly-Si fibers,¹⁶ nano-spike coupler,⁴³ and the rod-in-stack technique.²⁰ The upper half highlights some of the nonlinear processes that have been enabled by the advancements. First, in the amorphous core material: nonlinear transmission (SPM),²⁵ all-optical modulation: TPA²⁶ and XPM,²⁷ mid-infrared nonlinear transmission⁶³ FWM and supercontinuum generation.³² Second, in the tapered SCFs: microspherical resonator,⁶⁴ supercontinuum generation,³⁷ wavelength conversion,⁴⁴ optical parametric amplification,²⁹ broadband FWM,²⁸ Raman amplification,¹⁹ Raman-enhanced FWM,³⁰ frequency comb generation,⁴⁵ and undetected-photon imaging.³⁴

were retained on the SCF so that the input and output core diameters were $\sim 4 \mu\text{m}$. One can clearly see the benefits of reducing the losses and improving the coupling efficiency in terms of power handling and the achievable nonlinear phase shift.

It is worth noting that, owing to the large TPA parameter of silicon at telecom wavelengths, nonlinear saturation can limit the performance when using high peak powers. Although such saturation is normally undesirable, it can be exploited for use in all-optical modulation formats, e.g., where the presence of a high-power control beam is used to modulate the amplitude of a signal wave through increased absorption.²⁶ As the TPA process is governed by the electronic nonlinear response, the response time of the material is ultra-fast, so high-speed modulation is possible. However, in most nonlinear applications, TPA is best avoided, and this is greatly facilitated by reducing the linear losses so that the pump powers required to observe the desired nonlinear process are below the saturation level, as has been the focus of much of our work.²⁹

Following the initial nonlinear characterizations, several other processes were observed, including cross-phase modulation (XPM)²⁷ and FWM.³² Although XPM could be observed in large core SCFs, the key to observing FWM was to produce smaller core fibers that exhibited zero-dispersion wavelengths (ZDW) in the vicinity of available pump sources. Spontaneous FWM was first demonstrated in an a-Si:H core fiber with a $1.7 \mu\text{m}$ core diameter, such that a $2.3 \mu\text{m}$ pump was required to ensure proximity to the ZDW.³² Therefore, it was not until a low loss, submicron core

tapered SCF was produced until the first full characterization of parametric gain in the telecom band could be undertaken.²⁹ Specifically, the SCF had a poly-Si core with a diameter of 915 nm , over a length of 5 mm [design as in Fig. 4(b)], and a loss of 2.8 dB/cm , which represented the lowest transmission loss of a submicron core SCF at that time.

The results of the FWM characterization using a femtosecond pump and a tunable CW seed are shown in Fig. 5(a), where a broad conversion bandwidth of almost 300 nm was recorded. As a result of the combination of low coupling and transmission losses for this tapered SCF, a maximum on-off parametric gain of 9 dB was obtained, which was higher than comparable reports in planar silicon waveguides.³³ Using a similar SCF design, FWM-based wavelength conversion of 20 Gbit/s data signals via a 1550 nm CW pump was subsequently demonstrated over the extended telecommunications region, including the S-, C-, and L-bands, as confirmed by constellation diagrams and spectra in Fig. 5(b). More recently, FWM has also been used as a source of photon pairs for an undetected photon imaging scheme, where the signal beam interacts with the object while the idler is used for the detection,³⁴ thus highlighting the potential for these fibers to find application in a range of FWM-based processing applications.

The most recent nonlinear process to be reported in the SCFs is Raman scattering. Although Raman scattering was the first nonlinear process to be demonstrated in the planar silicon waveguides,³⁵ its observation in the poly-Si core fibers had been hindered by the relatively short lengths of the early tapered designs. Therefore, the ability

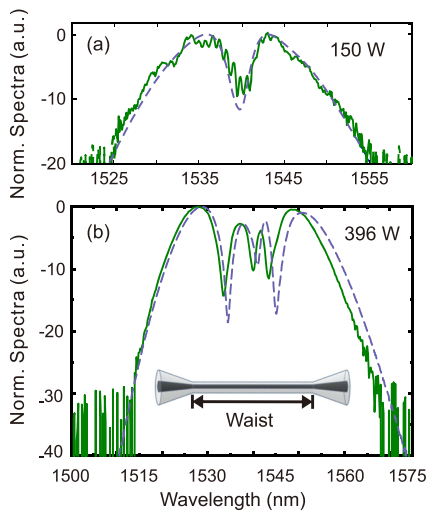


FIG. 4. SPM induced spectral broadening in two tapered poly-Si core fibers. (a) Early taper with a core diameter of $1\ \mu\text{m}$ and a loss of $3.5\ \text{dB/cm}$.¹⁶ (b) Taper optimized for improved coupling, as indicated in the inset, with a core of $0.9\ \mu\text{m}$ and a loss of $2.5\ \text{dB/cm}$. The powers labeled are peak powers for a pulsed pump source.

to observe a spontaneous Raman signal coincided with the production of tapered SCFs with losses of $\sim 1\ \text{dB/cm}$ over lengths of $\sim 2\ \text{cm}$, as illustrated in Fig. 6(a).¹⁹ This then led to the first demonstration of stimulated Raman amplification of a telecom signal, which was

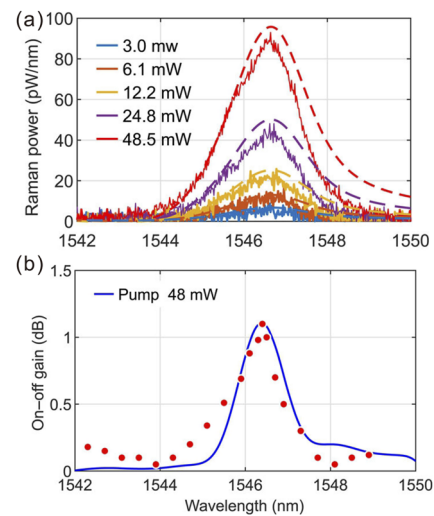


FIG. 6. (a) Spontaneous Raman emission spectra for a CW pump at $1431\ \text{nm}$ as recorded for different coupled powers.¹⁹ (b) Stimulated Raman gain for a $1431\ \text{nm}$ pump with a coupled power of $48\ \text{mW}$ as measured for various signal wavelengths.¹⁹

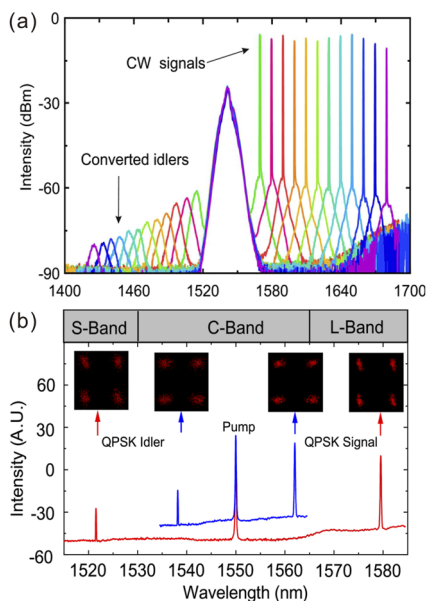


FIG. 5. (a) Transmission spectra taken at the output of the SCF as the signal wavelength is tuned from 1570 to $1680\ \text{nm}$.²⁹ (b) Measured spectra for wavelength conversion of $20\ \text{Gb/s}$ QPSK data at two signal wavelengths: 1563 and $1580\ \text{nm}$. The FWM spectra are offset by $10\ \text{dB}$. Insets show the constellation diagrams for the original and converted signals.²⁸

achieved using an SCF with a core diameter of $750\ \text{nm}$ and length of $1.9\ \text{cm}$, using a CW pump source at $1431\ \text{nm}$. With a coupled-in pump power of only $\sim 50\ \text{mW}$, an on-off gain of $1.1\ \text{dB}$ was achieved at the peak Raman frequency shift, as shown in Fig. 6(b). Significantly, this result represented the highest gain reported in silicon waveguides of comparable size using mW pump powers, which was attributed to the low transmission loss of the sub-micrometer sized SCFs. Moreover, simulations have predicted that the gain could reach as high as $6\ \text{dB}$ in a similar SCF with a length of $\sim 10\ \text{cm}$, which is comparable to the largest gains obtained in an SOI platform with a high power ($\sim 120\ \text{mW}$) CW pump,³⁶ and the gain could be further increased by reducing the losses.

Although the majority of nonlinear demonstrations in the SCFs have focused on the telecom band, the ability to produce high quality taper designs with core dimensions of several micrometers is advantageous for their application in the longer, mid-infrared wavelength region. Moreover, as the TPA parameter of silicon decreases with increasing pump wavelengths, becoming negligible beyond the TPA edge ($\sim 2.2\ \mu\text{m}$),³⁷ nonlinear absorption processes can be significantly reduced in this region, which allows for the use of higher power pumps. As seen in Fig. 2(b), an SCF with a core diameter of $\sim 3\ \mu\text{m}$ has a ZDW of around $2.8\ \mu\text{m}$, and simulations have shown that the propagation losses in such a large core fiber will remain below $1\ \text{dB/cm}$ for wavelengths up to $\sim 4.7\ \mu\text{m}$, with only a modest increase beyond this. Taking advantage of this, supercontinuum generation spanning almost two octaves (1.6 – $5.3\ \mu\text{m}$) has been demonstrated in a tapered SCF, illustrated in the sketch of Fig. 7(a), with a waist diameter of $2.8\ \mu\text{m}$, a length of $\sim 1\ \text{cm}$, and a loss of $\sim 1\ \text{dB/cm}$ at the $3\ \mu\text{m}$ pump wavelength.³⁸ The generation and transmission of the longest wavelengths shown in Fig. 7(b) were facilitated by the asymmetric taper design, where the slow input taper allowed for efficient coupling and optimized nonlinear conversion in the waist, while the fast output taper helped to

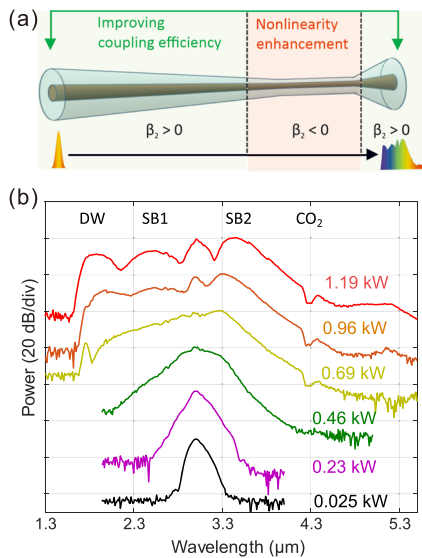


FIG. 7. (a) Schematic of the asymmetric taper design used for mid-infrared supercontinuum generation.³⁸ (b) Measured transmission spectra obtained for pumping the fiber design in (a) using a femtosecond OPO tuned to 3 μm for the average powers as labeled for a pulsed pump source.³⁸

reduce the interaction with the lossy silica cladding. As a result, the red edge of the broadest continuum spectrum (10 mW pump corresponding to a peak power of 1.19 kW) extends well beyond the previous cutoff of $\sim 3.3 \mu\text{m}$ obtained in a SOI waveguide (by $\sim 2 \mu\text{m}$).³⁹ Moreover, thanks to the low transmission losses and specifically the negligible TPA of the pump, a high conversion efficiency of $\sim 60\%$ was obtained, resulting in a supercontinuum source with sufficient power ($\sim 6 \text{ mW}$ average power) for use in state-of-the-art mid-infrared gas spectroscopy applications.⁴⁰ Significantly, further simulations of the mid-infrared transmission losses associated with the silica cladding have shown that, through the selection of an appropriate core size and fiber length, SCF devices can be designed to operate with high efficiency and low insertion losses over the entire transmission window of the core (1–8 μm).³⁸ Therefore, these results highlight the potential benefits of SCFs over their planar counterparts in terms of power handling and wavelength coverage spanning from the near to the mid-infrared.

III. HARNESSING THE FIBER GEOMETRY

A. All-fiber integrated telecom demonstrators

One of the key advantages of the SCF platform is its potential to be seamlessly linked to conventional silica fiber components to form robust and compact systems. However, integrating SCFs with all-silica fibers does present some challenges due to the large refractive index difference of the core materials, which results in mismatches in fiber core size, mode properties, and large reflection losses at the joint. Although preliminary efforts to integrate the SCF with standard single mode fibers (SMFs) showed that robust connections were possible as long as the fusion temperature was kept low,⁴¹ the large mode mismatch and high Fresnel reflection resulted in prohibitively large coupling losses. Subsequent work demonstrated that

it was possible to reduce the reflection losses via chemical etching of the core before splicing, though the mode mismatch contribution was still high.⁴² An alternative integration approach that allows for the reduction of coupling losses due to both reflection and mode mismatch is to fabricate nano-spike couplers onto the ends of the high index fiber core, as shown in the schematic of Fig. 8(a), similar to the inverse tapers employed in planar integrated photonics.⁴³ Such nano-spike couplers can be fabricated onto the end facets of the poly-Si fibers using a modified tapering procedure whereby the SCF is heated such that the silicon core collapses so that short spikes of length $\sim 200 \mu\text{m}$ appear at each end of the discontinuous fiber [see inset in Fig. 8(a)]. The SCF can then be cleaved in the section of the fiber with the collapsed core before splicing to an SMF that has also been tapered to have a matching outer cladding diameter, as shown in Fig. 8(b) and described in Ref. 44.

To confirm the viability of the nano-spike integration coupling scheme, an SCF with an SMF pigtail at the input facet was fabricated and demonstrated for use as a nonlinear wavelength converter of data signals in the telecom C-band.⁴⁵ This work showed that it was possible to produce a nano-spike coupler on the end of an SCF that had been pre-tapered to support FWM for a 1554 nm pump (transmission loss of $\sim 2 \text{ dB/cm}$ over a length of $\sim 1 \text{ cm}$). Significantly, the resulting coupling loss for the nano-spike of 4.5 dB was almost 50% lower than for coupling via a free-space launch into an SCF with a $\sim 1 \mu\text{m}$ core, where the typical input loss is $\sim 8 \text{ dB}$. This device was subsequently employed for the successful conversion of 20 Gb/s quadrature phase-shift keying (QPSK) signals with

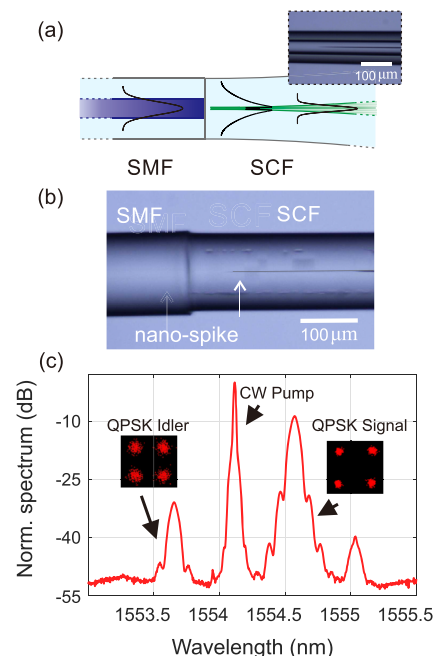


FIG. 8. (a) Mode evolution from SMF to tapered SCF. Inset: a microscope image of the fabricated nano-spike. (b) Microscope image of the splicing joint for the SCF–SMF connection. (c) FWM converted QPSK spectrum recorded at the output of the SMF coupled SCF. Signal and idler constellation diagrams are shown as insets.⁴⁵

a low optical signal-to-noise-ratio (OSNR) penalty, as illustrated by Fig. 8(c). More recently, the fabrication approach was extended to produce nano-spike couplers on both ends of the SCF, allowing for SMF pigtails at the input and output.⁴⁶ Although this was the first demonstration of a fully integrated SCF-SMF device, there were several challenges in fabricating the heterogeneous structure due to the short SCF length, which resulted in high coupling losses of ~ 8 dB per nano-spike. Nevertheless, the high optical quality of the SCF section still allowed for efficient nonlinear spectral broadening of a telecoms frequency comb to triple the bandwidth of the source (from 10 to 30 nm) while preserving key performance features such as comb flatness (12 dB), narrow comb linewidths (< 3 kHz), and low noise levels (> 30 dB OSNR).

Another potential application for the all-fiber SCF systems in the telecom band is, in fact, to harness the high-speed absorption properties associated with the large TPA (discussed in Sec. II) for the development of all-optical modulation schemes within the optical networks. However, so far the modulation performance of the SCFs has been hindered by the short fiber lengths and lack of SCF integration, so the required pumping schemes are impractical, particularly in terms of the power requirements. With the recent advancements in both the fabrication of long lengths of low loss tapered fibers and the nano-spike integration methods, all-fiber modulators can now be envisaged where both the pump and probe waves operate at power levels employed in conventional networks. Figure 9(a) presents a sketch of such a scheme, where the pump consists of a modulated 20 mW CW source at 1310 nm and the signal is a 10 mW CW probe at 1550 nm, as representative wavelengths commonly used

for wavelength division multiplexing (WDM) optical communications. Thanks to the ultrafast absorption of the TPA process, the modulated probe is produced as a precise dark copy of the pump, as displayed in Fig. 9(b), with a modulation depth that is determined by the fiber length and loss parameter. From Fig. 9(c), we see that for SCFs with losses in the range of 0.1–0.5 dB/cm, modulation depths between 0.5 and 1 dB can be achieved within a length of ~ 10 cm, which could be used for optical link monitoring in passive optical networks.⁴⁷ Compared to alternative approaches that make use of planar silicon waveguides,⁴⁸ the all-fiber system described here will not only help to ensure the robustness and stability of the networks but also keep the power consumption low.

B. Mid-infrared source generation

In contrast to the near-infrared region, where there are numerous competing waveguide platforms, components for the mid-infrared are in general less well developed. Therefore, there is considerable scope for the SCFs to have a significant impact in this regime, and especially for the generation of new sources via nonlinear conversion. Although there are other fiber materials that offer good transmission within the mid-infrared, such as chalcogenides, tellurite, and fluoride glasses, these typically suffer from poor chemical and mechanical stability, so the resulting fibers are fragile and have a limited lifetime, particularly when operated at high pump powers.⁴⁹ Moreover, the SCFs also offer benefits over traditional planar semiconductor waveguides as they can be fabricated to have large core sizes, which helps to increase their power handling capability, facilitate phase-matching for long wavelength pump sources, as well as reduce the interaction of the mid-infrared generated light with the lossy silica cladding, as already demonstrated via the supercontinuum spectrum in Fig. 7(b). However, for applications such as spectroscopy, metrology, and optical coherence tomography (OCT), it is often important to ensure that the generated supercontinuum can preserve the coherence of the pump laser.

To investigate this further, simulations of the nonlinear propagation in the asymmetric tapered SCF have been conducted using the same pump parameters as in the experiments but assuming a comb seed consisting of a stable train of pulses with a duration of ~ 100 fs (FWHM) and an 80 MHz repetition rate.³⁸ Figure 10(a) shows the calculated comb spectrum, which matches well with the previous experiments in terms of wavelength coverage and spectral features. Importantly, the simulations confirm that, as the supercontinuum is generated principally by the SPM and FWM processes, the coherence is defined by the pump source.⁵⁰ Close up views of two spectral regions confirm that the comb spans more than an octave in frequency, as shown in Figs. 10(b) and 10(c). The extinction ratios of the comb lines are found to be greater than 30 dB, which is suitable for high-precision spectroscopy applications. It is worth noting that the robustness and stability of the comb source would greatly benefit from integrating the pump directly with the SCF, as discussed earlier, which could be achieved using one of the emerging ~ 3 μm fiber laser systems.⁵¹

Although the current demonstrations have shown source generation extending over more than half of the transmission window of silicon, there is significant value in extending the wavelength coverage of the continuum spectrum closer to the long wavelength transmission edge of the core, where there are potential applications

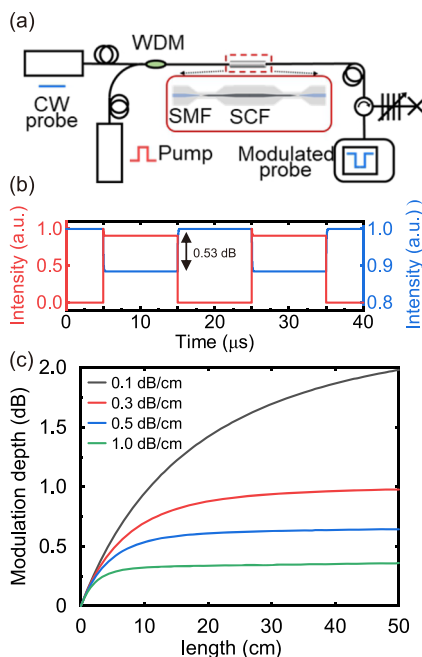


FIG. 9. (a) Schematic of in-line fiber-integrated nonlinear optical modulator. (b) Intensity of input pump and modulated probe at 1310 and 1550 nm, respectively. (c) Modulation depth as a function of SCF length under different linear losses.

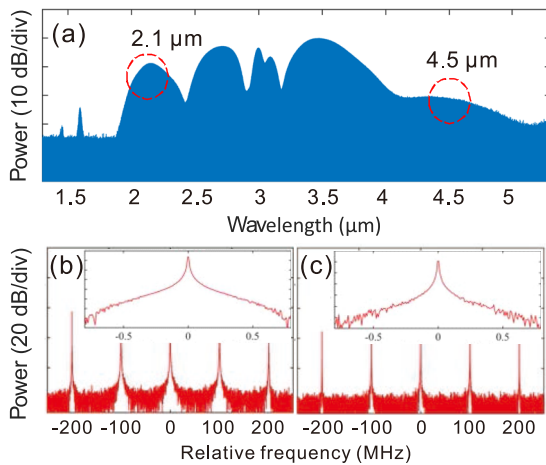


FIG. 10. (a) Simulated SCF-based frequency comb obtained with 10 000 input pulses and a repetition rate of 80 MHz. Close-up views of spectra simulated in the vicinity of (b) 2.1 μm and (c) 4.5 μm . The insets show a single comb line.

in security and industrial process monitoring.⁵² By further adjusting the tapered SCF profile to focus on the generation of the longer wavelength signals, simulations have shown that it is possible to extend the red spectral components of the supercontinuum out to $\sim 8 \mu\text{m}$. The main features of the new design are that the tapered waist diameter is slightly increased to 3.1 μm and the overall fiber length is shortened to 6.7 mm, which helps to minimize the interaction of the mid-infrared light with the cladding and reduce transmission losses. More specifically, the SCF is designed to gradually taper down from an input diameter of $\sim 7.3 \mu\text{m}$ over a length of $\sim 4 \text{ mm}$ to reach a waist with a diameter of $\sim 3.1 \mu\text{m}$ and a length of $\sim 1.4 \text{ mm}$, which allows for a gradual evolution of red-shifted generated light from which to seed the supercontinuum. This is then followed by a short, $\sim 1.2 \text{ mm}$ inverse taper up to an output diameter of $\sim 9.3 \mu\text{m}$, as illustrated in Fig. 11(a). The resulting spectral broadening is displayed in Fig. 11(b), with the total bandwidth (1.9–8 μm) covering $\sim 90\%$ of the transmission window of the core. As most of the red-shifted wavelengths are in fact generated in the output taper, this ensures that

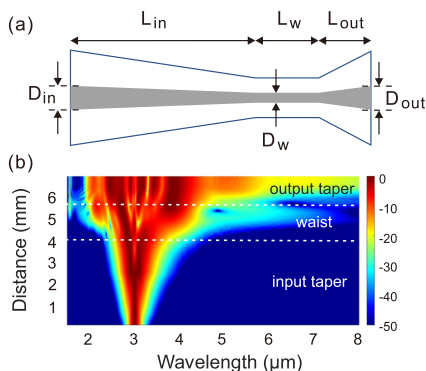


FIG. 11. (a) Schematic of the asymmetric taper design. (b) Simulated broadband supercontinuum generation covering 2–8 μm using the SCF platform.

any loss due to the interaction with the silica cladding is minimal so that practical output powers can be achieved with an appropriate pump source. In particular, for an increased average pump power of $\sim 30 \text{ mW}$ (corresponding to a peak power of 3 kW) as used here, we predict that supercontinuum powers as high as $\sim 20 \text{ mW}$ could be achieved via this scheme.

Finally, it is also worth mentioning that, in addition to broadband source generation, tunable, narrow-band mid-infrared sources could be developed using the SCFs by exploiting the large Raman gain coefficient of the crystalline core material.⁵³ Significantly, although a cascaded Raman laser capable of operating out to 1.8 μm has been demonstrated using an integrated silicon resonator, so far there have been no observations of Raman amplification in silicon waveguides beyond 2 μm . The ability to develop all-fiber integrated SCF systems that could support high power and wavelength tunable operation across the 2–3 μm regime would thus be highly advantageous for many applications spanning sensing, medical diagnostics, and environmental monitoring.

IV. PERSPECTIVES AND CHALLENGES

The advancements made in the production of increasingly long lengths of low loss SCFs are opening up exciting prospects for their nonlinear application. However, there is still more work to be performed, as outlined below.

A. Loss reduction and material choice

Although the current post-processing and two-step drawing techniques can produce SCFs with losses around $\sim 0.2 \text{ dB/cm}$,^{20,37} driving the losses down further to $\sim 1 \text{ dB/m}$ would be transformative for improving their practicality in terms of increasing the useable fiber lengths and reducing the power requirements. We also expect that such loss reductions will open up new areas of application for the SCFs, such as in the delivery of long wavelength sources for medical probes and surgery or for quantum information processing, where every generated photon is precious. In our view, the most likely route to achieving such low losses will come from combining aspects of the various fabrication methods employed by the different groups. For example, the rod-in-stack method could be combined with post-processing procedures such as tapering to further control the polycrystalline grain size, while the inclusion of an interface modifier in this method could help to reduce contamination or residual strain in the core.

In addition to this, the potential to include other semiconductor core materials within the fiber structure will also help to expand the functionality and wavelength coverage of this platform. To date, fibers have been made with various semiconductor core materials, including germanium,⁵⁴ tellurium,⁵⁵ ZnSe,⁵⁶ GaAs,²³ and SiGe alloys.²² Of these fibers, the SiGe material system offers the most immediate promise for nonlinear applications, as the fabrication methods are well suited to the post-processing techniques discussed earlier, and thus there is a clear route for the production of low loss fibers. Moreover, compared to pure silicon, SiGe can offer higher nonlinear coefficients and longer mid-infrared wavelength coverage, and it is also possible to tune its optical properties through the composition of the constituents to match the target application.⁵⁷ However, it is worth noting that any advancements to the fabrication

of the compound semiconductor core fibers such as ZnSe and GaAs to improve the optical quality would be hugely exciting, not only from a nonlinear perspective as it would allow access to large, in-fiber second order nonlinear coefficients⁵⁸ but also for the potential development of in-fiber laser systems.⁵⁹ Determining and eliminating sources of transmission loss in these materials is thus a critical goal for future studies.

B. Low loss integration from near infrared to the mid-IR

As we have discussed, the ability to robustly connect the SCFs with more conventional glass fibers is important not only to reduce the losses at the connection points but also to improve the robustness and handleability of the SCF systems. Unfortunately, initial attempts to splice SMF to both ends of an SCF resulted in high losses (8 dB per facet) due to the non-optimal design. However, simulations have shown that these losses could be reduced to ~1 dB by adjusting the nano-spike length and outer cladding diameter, as displayed in Fig. 12. However, in order to achieve such designs, it is likely that as-drawn SCFs will need to be fabricated with different core/cladding ratios to support the tapering down to such small cladding diameters.

Moreover, integration should also be explored for direct connection to fibers that operate in the mid-infrared region (2–8 μm), such as hollow core microstructured fibers⁶⁰ or commercially available fluoride fibers. As silica has high losses for operations $>2.3 \mu\text{m}$, larger core SCFs will be needed at the connection joint in order to minimize interaction with the silica cladding. Therefore, alternative mechanisms for low loss coupling will need to be explored that reduce both the reflection losses and mode-mismatch of the different fiber systems. Therefore, it would be worth revisiting some of the previous splicing procedures used for the large core SCFs that made use of chemical etching to reduce the reflections,⁴¹ as well as exploring new schemes that make use of angle cleaving.⁶¹ However, whatever the method employed, the focus should remain on ensuring the integrated systems are robust, stable, and easy to handle, thus facilitating their use across a wide range of research areas.

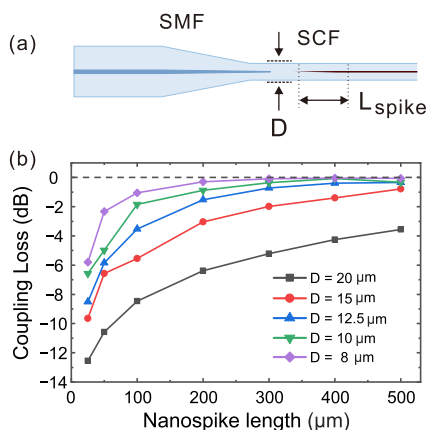


FIG. 12. (a) Schematic of the SMF-SCF splicing joint with a nano-spike coupler. (b) A plot of coupling loss vs nanospoke length for different cladding diameters.

V. CONCLUDING REMARKS

This study has reviewed progress in the fabrication and post-processing of the silicon core fibers with a view to unlocking their potential for use in nonlinear optical applications. The significant advancements that have been made in terms of reducing the transmission losses, controlling the core diameter, and increasing the useable fiber lengths have enabled a multitude of nonlinear processes to be explored from the simplest case of nonlinear absorption saturation to phase-matched FWM and extreme supercontinuum generation. Over the forthcoming years, we anticipate the efforts will continue to focus on loss reduction, both in terms of improving the optical transmission quality of the core materials and their interconnection with other glass-based fiber components. Such advancements will be critical for increasing the employment of the SCFs in practical systems as well as opening up new and exciting areas of exploration spanning the near to mid-infrared wavelength regimes.

ACKNOWLEDGMENTS

The authors acknowledge their colleagues who have provided valuable contributions to the cited work, particularly P. Mehta, N. Healy, F. Suhailin, Y. Franz, T. Hawkins, U. J. Gibson, and J. Ballato. This work was supported by the Engineering and Physical Sciences Research Council (Grant No. EP/P000940/1) and the National Natural Science Foundation of China (Grant No. 62175080).

AUTHOR DECLARATIONS

Conflict of Interest

The authors have no conflicts to disclose.

Author Contributions

Li Shen: Conceptualization (supporting); Formal analysis (supporting); Supervision (supporting); Writing – original draft (equal); Writing – review & editing (equal). **Meng Huang:** Formal analysis (supporting); Investigation (supporting); Visualization (supporting); Writing – review & editing (supporting). **Shiyu Sun:** Formal analysis (supporting); Investigation (supporting); Writing – review & editing (supporting). **Dong Wu:** Formal analysis (supporting); Investigation (supporting); Writing – review & editing (supporting). **Zhiwei Yan:** Formal analysis (supporting); Investigation (supporting); Writing – review & editing (supporting). **Haonan Ren:** Formal analysis (supporting); Investigation (supporting); Visualization (supporting); Writing – review & editing (supporting). **Anna C. Peacock:** Conceptualization (lead); Formal analysis (equal); Funding acquisition (lead); Supervision (lead); Writing – original draft (equal); Writing – review & editing (equal).

DATA AVAILABILITY

The data that support the findings of this study are available from the corresponding authors upon reasonable request.

REFERENCES

- ¹B. Jalali and S. Fathpour, "Silicon photonics," *J. Lightwave Technol.* **24**, 4600–4615 (2006).
- ²P. Dong, Y.-K. Chen, G.-H. Duan, and D. T. Neilson, "Silicon photonic devices and integrated circuits," *Nanophotonics* **3**, 215–228 (2014).
- ³J. Leuthold, C. Koos, and W. Freude, "Nonlinear silicon photonics," *Nat. Photonics* **4**, 535–544 (2010).
- ⁴C. Koos, L. Jacome, C. Poulton, J. Leuthold, and W. Freude, "Nonlinear silicon-on-insulator waveguides for all-optical signal processing," *Opt. Express* **15**, 5976–5990 (2007).
- ⁵B. Kuyken, T. Ideguchi, S. Holzner, M. Yan, T. W. Hänsch, J. Van Campenhout, P. Verheyen, S. Coen, F. Leo, R. Baets, G. Roelkens, and N. Picqué, "An octave-spanning mid-infrared frequency comb generated in a silicon nanophotonic wire waveguide," *Nat. Commun.* **6**, 6310 (2015).
- ⁶H. Rong, A. Liu, R. Jones, O. Cohen, D. Hak, R. Nicolaescu, A. Fang, and M. Paniccia, "An all-silicon Raman laser," *Nature* **433**, 292–294 (2005).
- ⁷J. Ballato, T. Hawkins, P. Foy, R. Stolen, B. Kokuoz, M. Ellison, C. McMillen, J. Reppert, A. M. Rao, M. Daw, S. Sharma, R. Shori, O. Stafsudd, R. R. Rice, and D. R. Powers, "Silicon optical fiber," *Opt. Express* **16**, 18675–18683 (2008).
- ⁸N. Healy, J. R. Sparks, P. J. A. Sazio, J. V. Badding, and A. C. Peacock, "Tapered silicon optical fibers," *Opt. Express* **18**, 7596–7601 (2010).
- ⁹Y. Franz, A. F. J. Runge, H. Ren, N. Healy, K. Ignatyev, M. Jones, T. Hawkins, J. Ballato, U. J. Gibson, and A. C. Peacock, "Material properties of tapered crystalline silicon core fibers," *Opt. Mater. Express* **7**, 2055–2061 (2017).
- ¹⁰P. J. A. Sazio, A. Amezcua-Correa, C. E. Finlayson, J. R. Hayes, T. J. Scheidemantel, N. F. Baril, B. R. Jackson, D.-J. Won, F. Zhang, E. R. Margine, V. Gopalan, V. H. Crespi, and J. V. Badding, "Microstructured optical fibers as high-pressure microfluidic reactors," *Science* **311**, 1583 (2006).
- ¹¹S. Morris, C. McMillen, T. Hawkins, P. Foy, R. Stolen, J. Ballato, and R. Rice, "The influence of core geometry on the crystallography of silicon optical fiber," *J. Cryst. Growth* **352**, 53–58 (2012).
- ¹²N. F. Baril, R. He, T. D. Day, J. R. Sparks, B. Keshavarzi, M. Krishnamurthi, A. Borhan, V. Gopalan, A. C. Peacock, N. Healy, P. J. A. Sazio, and J. V. Badding, "Confined high-pressure chemical deposition of hydrogenated amorphous silicon," *J. Am. Chem. Soc.* **134**, 19–22 (2012).
- ¹³E. F. Nordstrand, A. N. Dibbs, A. J. Eraker, and U. J. Gibson, "Alkaline oxide interface modifiers for silicon fiber production," *Opt. Mater. Express* **3**, 651–657 (2013).
- ¹⁴A. C. Peacock, U. J. Gibson, and J. Ballato, "Silicon optical fibres—past, present, and future," *Adv. Phys.: X* **1**, 114–127 (2016).
- ¹⁵S. Chaudhuri, J. R. Sparks, X. Ji, M. Krishnamurthi, L. Shen, N. Healy, A. C. Peacock, V. Gopalan, and J. V. Badding, "Crystalline silicon optical fibers with low optical loss," *ACS Photonics* **3**, 378–384 (2016).
- ¹⁶F. H. Suhailin, L. Shen, N. Healy, L. Xiao, M. Jones, T. Hawkins, J. Ballato, U. J. Gibson, and A. C. Peacock, "Tapered polysilicon core fibers for nonlinear photonics," *Opt. Lett.* **41**, 1360–1363 (2016).
- ¹⁷N. Healy, M. Fokine, Y. Franz, T. Hawkins, M. Jones, J. Ballato, A. C. Peacock, and U. J. Gibson, "CO₂ laser-induced directional recrystallization to produce single crystal silicon-core optical fibers with low loss," *Adv. Opt. Mater.* **4**, 1004–1008 (2016).
- ¹⁸A. C. Peacock, "Soliton propagation in tapered silicon core fibers," *Opt. Lett.* **35**, 3697–3699 (2010).
- ¹⁹M. Huang, S. Sun, D. Wu, H. Ren, L. Shen, T. W. Hawkins, J. Ballato, U. J. Gibson, and A. C. Peacock, "Continuous-wave Raman amplification in silicon core fibers pumped in the telecom band," *APL Photonics* **6**, 096105 (2021).
- ²⁰M. Kudina, G. Bouwmans, O. Vanvincq, R. Habert, S. Plus, R. Bernard, K. Baudelle, A. Cassez, B. Chazallon, M. Marinova, N. Nuns, and L. Bigot, "Two-step manufacturing of hundreds of meter-long silicon micrometer-size core optical fibers with less than 0.2 dB/cm background losses," *APL Photonics* **6**, 026101 (2021).
- ²¹N. Healy, S. Mailis, N. M. Bulgakova, P. J. A. Sazio, T. D. Day, J. R. Sparks, H. Y. Cheng, J. V. Badding, and A. C. Peacock, "Extreme electronic bandgap modification in laser-crystallized silicon optical fibres," *Nat. Mater.* **13**, 1122–1127 (2014).
- ²²D. A. Coucheron, M. Fokine, N. Patil, D. W. Breiby, O. T. Buset, N. Healy, A. C. Peacock, T. Hawkins, M. Jones, J. Ballato, and U. J. Gibson, "Laser recrystallization and inscription of compositional microstructures in crystalline SiGe-core fibres," *Nat. Commun.* **7**, 13265 (2016).
- ²³T. Zaengle, U. J. Gibson, T. W. Hawkins, C. McMillen, B. Ghimire, A. M. Rao, and J. Ballato, "A novel route to fibers with incongruent and volatile crystalline semiconductor cores: GaAs," *ACS Photonics* **9**, 1058–1064 (2022).
- ²⁴U. J. Gibson, L. Wei, and J. Ballato, "Semiconductor core fibres: Materials science in a bottle," *Nat. Commun.* **12**, 3990 (2021).
- ²⁵P. Mehta, N. Healy, N. F. Baril, P. J. A. Sazio, J. V. Badding, and A. C. Peacock, "Nonlinear transmission properties of hydrogenated amorphous silicon core optical fibers," *Opt. Express* **18**, 16826–16831 (2010).
- ²⁶P. Mehta, N. Healy, T. D. Day, J. R. Sparks, P. J. A. Sazio, J. V. Badding, and A. C. Peacock, "All-optical modulation using two-photon absorption in silicon core optical fibers," *Opt. Express* **19**, 19078–19083 (2011).
- ²⁷P. Mehta, N. Healy, T. D. Day, J. V. Badding, and A. C. Peacock, "Ultrafast wavelength conversion via cross-phase modulation in hydrogenated amorphous silicon optical fibers," *Opt. Express* **20**, 26110–26116 (2012).
- ²⁸D. Wu, L. Shen, H. Ren, M. Huang, C. Lacava, J. Campling, S. Sun, T. W. Hawkins, U. J. Gibson, P. Petropoulos, J. Ballato, and A. C. Peacock, "Four-wave mixing-based wavelength conversion and parametric amplification in submicron silicon core fibers," *IEEE J. Sel. Top. Quantum Electron.* **27**, 4300111 (2021).
- ²⁹D. Wu, L. Shen, H. Ren, J. Campling, T. W. Hawkins, J. Ballato, U. J. Gibson, and A. C. Peacock, "Net optical parametric gain in a submicron silicon core fiber pumped in the telecom band," *APL Photonics* **4**, 086102 (2019).
- ³⁰S. Sun, M. Huang, D. Wu, L. Shen, H. Ren, T. W. Hawkins, J. Ballato, U. J. Gibson, G. Z. Mashanovich, and A. C. Peacock, "Raman enhanced four-wave mixing in silicon core fibers," *Opt. Lett.* **47**, 1626–1629 (2022).
- ³¹S. Hong, L. Zhang, Y. Wang, M. Zhang, Y. Xie, and D. Dai, "Ultralow-loss compact silicon photonic waveguide spirals and delay lines," *Photonics Res.* **10**, 1–7 (2022).
- ³²L. Shen, N. Healy, L. Xu, H. Y. Cheng, T. D. Day, J. H. V. Price, J. V. Badding, and A. C. Peacock, "Four-wave mixing and octave-spanning supercontinuum generation in a small core hydrogenated amorphous silicon fiber pumped in the mid-infrared," *Opt. Lett.* **39**, 5721–5724 (2014).
- ³³M. A. Foster, A. C. Turner, J. E. Sharping, B. S. Schmidt, M. Lipson, and A. L. Gaeta, "Broad-band optical parametric gain on a silicon photonic chip," *Nature* **441**, 960–963 (2006).
- ³⁴M. Huang, D. Wu, H. Ren, L. Shen, T. W. Hawkins, J. Ballato, U. J. Gibson, M. Beresna, R. Slavik, J. E. Sipe, M. Liscidini, and A. C. Peacock, "Classical imaging with undetected photons using four-wave mixing in silicon core fibers," *Photonics Res.* **11**, 137–142 (2023).
- ³⁵R. Claps, D. Dimitropoulos, V. Raghunathan, Y. Han, and B. Jalali, "Observation of stimulated Raman amplification in silicon waveguides," *Opt. Express* **11**, 1731–1739 (2003).
- ³⁶M. Ahmadi, J. Lefebvre, W. Shi, and S. LaRochelle, "Non-reciprocal sub-micron waveguide Raman amplifiers, towards loss-less silicon photonics," *IEEE J. Sel. Top. Quantum Electron.* **29**, 6100108 (2023).
- ³⁷H. Ren, L. Shen, D. Wu, O. Aktas, T. Hawkins, J. Ballato, U. J. Gibson, and A. C. Peacock, "Nonlinear optical properties of polycrystalline silicon core fibers from telecom wavelengths into the mid-infrared spectral region," *Opt. Mater. Express* **9**, 1271–1279 (2019).
- ³⁸H. Ren, L. Shen, A. F. J. Runge, T. W. Hawkins, J. Ballato, U. Gibson, and A. C. Peacock, "Low-loss silicon core fibre platform for broadband nonlinear photonics in the mid-infrared," *Light Sci. Appl.* **8**, 105 (2019).
- ³⁹N. Singh, M. Xin, D. Vermeulen, K. Shtyrkova, N. Li, P. T. Callahan, E. S. Magden, A. Ruocco, N. Fahrenkopf, C. Baiocco, B. P. Kuo, S. Radic, E. Ippen, F. X. Kärtner, and M. R. Watts, "Octave-spanning coherent supercontinuum generation in silicon on insulator from 1.06 μm to beyond 2.4 μm ," *Light Sci. Appl.* **7**, 17131 (2018).
- ⁴⁰D. Grassani, E. Tagkoudi, H. Guo, C. Herkommer, F. Yang, T. J. Kippenberg, and C.-S. Brès, "Mid infrared gas spectroscopy using efficient fiber laser driven photonic chip-based supercontinuum," *Nat. Commun.* **10**, 1553 (2019).
- ⁴¹L. Xiao, N. Healy, U. Gibson, T. Hawkins, M. Jones, J. Ballato, and A. C. Peacock, "Fusion splicing of silicon optical fibres," in CLEO/Europe-EQEC, Munich, 2015.

- ⁴²J.-H. Chen, Y.-T. Sun, and L. A. Wang, "Reducing splicing loss between a silicon-cored optical fiber and a silica optical fiber," *IEEE Photonics Technol. Lett.* **28**, 1774–1777 (2016).
- ⁴³V. R. Almeida, R. R. Panepucci, and M. Lipson, "Nanotaper for compact mode conversion," *Opt. Lett.* **28**, 1302–1304 (2003).
- ⁴⁴H. Ren, O. Aktas, Y. Franz, A. F. J. Runge, T. Hawkins, J. Ballato, U. J. Gibson, and A. C. Peacock, "Tapered silicon core fibers with nano-spikes for optical coupling via spliced silica fibers," *Opt. Express* **25**, 24157–24163 (2017).
- ⁴⁵M. Huang, H. Ren, O. Aktas, L. Shen, J. Wang, T. W. Hawkins, J. Ballato, U. J. Gibson, and A. C. Peacock, "Fiber integrated wavelength converter based on a silicon core fiber with a nano-spike coupler," *IEEE Photonics Technol. Lett.* **31**, 1561–1564 (2019).
- ⁴⁶R. Sohanpal, H. Ren, L. Shen, C. Deakin, A. M. Heidt, T. W. Hawkins, J. Ballato, U. J. Gibson, A. C. Peacock, and Z. Liu, "All-fibre heterogeneously-integrated frequency comb generation using silicon core fibre," *Nat. Commun.* **13**, 31637 (2022).
- ⁴⁷A. Usman, N. Zulkifli, M. R. Salim, K. Khairi, and A. I. Azmi, "Optical link monitoring in fibre-to-the-x passive optical network (FTTx PON): A comprehensive survey," *Opt. Switching Networking* **39**, 100596 (2020).
- ⁴⁸V. R. Almeida, C. A. Barrios, R. R. Panepucci, and M. Lipson, "All-optical control of light on a silicon chip," *Nature* **431**, 1081–1084 (2004).
- ⁴⁹Y. Ohishi, "Supercontinuum generation and IR image transportation using soft glass optical fibers: A review [invited]," *Opt. Mater. Express* **12**, 3990–4046 (2022).
- ⁵⁰J. M. Dudley and S. Coen, "Numerical simulations and coherence properties of supercontinuum generation in photonic crystal and tapered optical fibers," *IEEE J. Sel. Top. Quantum Electron.* **8**, 651–659 (2002).
- ⁵¹S. D. Jackson, "Towards high-power mid-infrared emission from a fibre laser," *Nat. Photonics* **6**, 423–431 (2012).
- ⁵²N. Picqué and T. W. Hänsch, "Mid-IR spectroscopic sensing," *Opt. Photonics News* **30**, 26–33 (2019).
- ⁵³V. Raghunathan, D. Borlaug, R. R. Rice, and B. Jalali, "Demonstration of a mid-infrared silicon Raman amplifier," *Opt. Express* **15**, 14355–14362 (2007).
- ⁵⁴J. Ballato, T. Hawkins, P. Foy, B. Yazgan-Kokuoz, R. Stolen, C. McMillen, N. K. Hon, B. Jalali, and R. Rice, "Glass-clad single-crystal germanium optical fiber," *Opt. Express* **17**, 8029–8035 (2009).
- ⁵⁵G. Tang, Q. Qian, X. Wen, G. Zhou, X. Chen, M. Sun, D. Chen, and Z. Yang, "Phosphate glass-clad tellurium semiconductor core optical fibers," *J. Alloys Compd.* **633**, 1–4 (2015).
- ⁵⁶J. R. Sparks, R. He, N. Healy, M. Krishnamurthi, A. C. Peacock, P. J. A. Sazio, V. Gopalan, and J. V. Badding, "Zinc selenide optical fibers," *Adv. Mater.* **23**, 1647–1651 (2011).
- ⁵⁷M. Montesinos-Ballester, C. Lafforgue, J. Frigerio, A. Ballabio, V. Vakarín, Q. Liu, J. M. Ramirez, X. Le Roux, D. Bouville, A. Barzaghi, C. Alonso-Ramos, L. Vivien, G. Isella, and D. Marris-Morini, "On-chip mid-infrared supercontinuum generation from 3 to 13 μm wavelength," *ACS Photonics* **7**, 3423 (2020).
- ⁵⁸N. Vukovic, N. Healy, J. R. Sparks, J. V. Badding, P. Horak, and A. C. Peacock, "Tunable continuous wave emission via phase-matched second harmonic generation in a ZnSe microcylindrical resonator," *Sci. Rep.* **5**, 11798 (2015).
- ⁵⁹M. G. Coco, S. C. Aro, S. A. McDaniel, A. Hendrickson, J. P. Krug, P. J. Sazio, G. Cook, V. Gopalan, and J. V. Badding, "Continuous wave Fe^{2+} :ZnSe mid-IR optical fiber lasers," *Opt. Express* **28**, 30263–30274 (2020).
- ⁶⁰H. C. H. Mulvad, S. Abokhamis Mousavi, V. Zuba, L. Xu, H. Sakr, T. D. Bradley, J. R. Hayes, G. T. Jasion, E. Numkam Fokoua, A. Taranta, S.-U. Alam, D. J. Richardson, and F. Poletti, "Kilowatt-average-power single-mode laser light transmission over kilometre-scale hollow-core fibre," *Nat. Photonics* **16**, 448–453 (2022).
- ⁶¹C. Zhang, E. N. Fokoua, S. Fu, M. Ding, F. Poletti, D. J. Richardson, and R. Slavik, "Angle-spliced SMF to hollow core fiber connection with optimized back-reflection and insertion loss," *J. Lightwave Technol.* **40**, 6474–6479 (2022).
- ⁶²N. Healy, S. Mailis, T. D. Day, P. J. Sazio, J. V. Badding, and A. C. Peacock, "Laser annealing of amorphous silicon core optical fibers," in *Specialty Optical Fibers*, OSA Technical Digest (Optical Society of America, 2012), p. STu1D.1.
- ⁶³L. Shen, N. Healy, P. Mehta, T. D. Day, J. R. Sparks, J. V. Badding, and A. C. Peacock, "Nonlinear transmission properties of hydrogenated amorphous silicon core fibers towards the mid-infrared regime," *Opt. Express* **21**, 13075–13083 (2013).
- ⁶⁴F. H. Suhailin, N. Healy, Y. Franz, M. Sumetsky, J. Ballato, A. N. Dibbs, U. J. Gibson, and A. C. Peacock, "Kerr nonlinear switching in a hybrid silica-silicon microspherical resonator," *Opt. Express* **23**, 17263–17268 (2015).